ACADEMIC PRESS

Available online at www.sciencedirect.com

SCIENCE DIRECT®

Journal of Sound and Vibration 261 (2003) 465–481

JOURNAL OF SOUND AND VIBRATION

www.elsevier.com/locate/jsvi

An adaptive beam model and dynamic characteristics of magnetorheological materials

Qing Sun*, Jin-Xiong Zhou, Ling Zhang

Department of Engineering Mechanics, Xi'an Jiaotong University, Xian Ning Road 28, Xian 710049, China

Received 23 October 2001; accepted 23 May 2002

Abstract

Magnetorheological (MR) materials show variations in their rheological properties when subjected to varying magnetic fields. They have quick time response, in the order of milliseconds, and thus are potentially applicable to structures and devices when a tunable system response is required. When incorporated into an adaptive structural system, they can yield higher variations in the dynamic response of the structure. This study presents a detailed analysis of dynamic characteristics of adaptive beam based on MR materials. The relationship between the magnetic field and the complex shear modulus of MR materials in the pre-yield regime is researched using oscillatory rheometry techniques. A structural dynamic modelling approach is discussed and vibration characteristics of MR adaptive structures are predicted for different magnetic field levels. In addition to the model predictions, actual MR adaptive beam is fabricated and tested. Both studies illustrate the vibration minimization capabilities of the MR adaptive beam at different magnetic field levels.
© 2002 Elsevier Science Ltd. All rights reserved.

1. Introduction

The dynamic behaviors of flexible beams, plates and shells are critical to the effective operation of many structures such as automobiles, aircrafts and space platforms. With appropriate control, fatigue failure can be avoided and undesirable resonance can be eliminated. Passive damping treatments have been successfully applied to various structures to attenuate their vibration response and eliminate vibration-induced noise.

In recent years, attention has been directed towards the use of various active and semi-active damping treatments. Distinct among these treatments are those in which controllable fluids are

*Corresponding author. Tel.: +86-29-254-5369; fax: +86-29-266-8301.
E-mail address: sqwxh@263.net (Q. Sun).

0022-460X/03/$ - see front matter © 2002 Elsevier Science Ltd. All rights reserved.
PII: S0022-460X(02)00985-9

used that are embedded in a laminated composite to control its vibration. Electrorheological (ER) materials and magnetorheological (MR) materials, due to their semi-active control capabilities, are candidate materials, which can cause changes in both damping and stiffness of the structure simultaneously. Their utilization in proposed applications is based on the concept of optimized control with minimum energy addition via semi-active control. While studies involving ER material based adaptive structures have been continuing over the past decade, the MR material based adaptive structures are in their initial research state. With currently attractive and steadily improving properties, ER and MR materials show promise for their use in adaptive structural applications in the future.

The development of ER material based adaptive structures was initiated during the past decade. As one of the earlier groups working in the area, Gandhi et al. [1,2] completed an experimental study on a variety of shear configuration based beam structures. A finite-element model was developed to simulate the controllable structure behavior. Choi et al. [3,4] also experimentally studied beam specimens subjected to cantilever-type boundary conditions, and observed a significant effect of electrical field on the vibration response. Mahjoob et al. [5] experimentally and theoretically studied composite beams filled with ER material under cantilever boundary conditions. They used a discretized model to predict the mechanical properties of the composite beams, and developed a methodology to extract the complex modulus of the ER layer from modal parameters of the beam.

In another study, Kordonsky et al. [6] experimentally investigated ER beam structures. The ER beam structure with cantilever end conditions was studied as structural and environmental conditions such as temperature, electrical field level and ER damping layer thickness level were varied. In the experiments, the shear storage modulus and loss factor of the ER material were calculated using an experimental method based on RKU theory [7]. Rahn and Joshi [8] developed an analytical model to predict and control the vibration response of ER adaptive beam structures. Their modelling study was based on the energy method. They presented expressions for different kinetic and potential energies due to shearing, bending and displacement.

Oyadiji [9] completed studies on composite structures filled with ER materials. Vibration responses of these structures were measured experimentally at different electric field levels and temperature levels, variations in responses were observed. Additionally, a theoretical model was developed, natural frequencies and loss factors were predicted, and a good agreement with the experiments was observed. Berg et al. [10] have completed another experimental study of composite beams filled with ER materials, and tested their responses at low voltage levels. Development of a theoretical model based on a microstructure behavior hypothesis was suggested. Yalcintas and Coulter [11,12] utilized ER materials as controllable stiffness damping layers and extended MM model [13] for homogeneous and non-homogeneous adaptive beam and plate configurations incorporating embedded sensors and neural network control mechanisms.

More recently, Choi et al. [14] exhibited a proof-of-concept investigation on vibration control of a cantilevered beam consisting of an ER fluid actuator (ERFA) and piezoelectric film actuator (PFA). A hybrid smart structure was fabricated and control schemes for ERFA and PFA were synthesized on the basis of field-dependent frequency responses and natural networks, respectively. Vibration performances in view of the suppression of tip deflections were evaluated to demonstrate the control effectiveness of the hybrid actuation methodology. In another study, Choi et al. [15] experimentally obtained noise control results of a rectangular closed cabin

featuring ER fluid-based smart plate on one side. Fuzzy control logic was formulated on the basis of field-dependent sound pressure levels of the cabin. The control logic was empirically realized and noise control results in the closed cabin were presented in both frequency and time domains.

In this paper, the relationship between the magnetic field and the complex shear modulus of MR materials in the pre-yield regime is researched using oscillatory rheometry techniques. A structural dynamic modelling approach is discussed and vibration characteristics of MR adaptive structures are predicted for different magnetic field levels. In addition to the model predictions, actual MR adaptive beam is fabricated and tested. Both studies illustrate the vibration minimization capabilities of the MR adaptive beam at different magnetic field levels. The result can be useful in a semi-active control.

2. MR fluid field-dependent complex shear modulus

MR fluids are in liquid form when there are no external stimuli. However, when they are subjected to an applied magnetic field, their physical appearance changes to become more like a solid gel. During this transformation, their rheological properties change as well. Fig. 1 is a schematic drawing of stress–strain behavior of MR materials for a varying range of magnetic fields. The peak values in Fig. 1 represent the static shear yield strength of the materials. As can be noticed in the figure, MR materials rheological response changes before and after the yield point. Due to this difference in the rheological behavior before and after the yield point, the MR rheology is modelled in pre- and post-yield regimes. Since the MR materials have higher stiffness values compared to ER materials, in their adaptive structures applications, the shear stresses experienced remain in the pre-yield regime. Therefore, the model considered in this study is based on pre-yield rheological properties of MR materials.

In the pre-yield regime, the MR materials demonstrate viscoelastic behavior. This viscoelastic behavior of the MR materials is analyzed by linear viscoelastic theories. As presented in Eq. (1), in the pre-yield regime, the shear stress τ is related to shear strain γ by complex shear modulus G^*:

$$\tau = G^*\gamma. \tag{1}$$

The complex shear modulus G^* is written in the form

$$G^* = G' + G''\mathrm{i}, \tag{2}$$

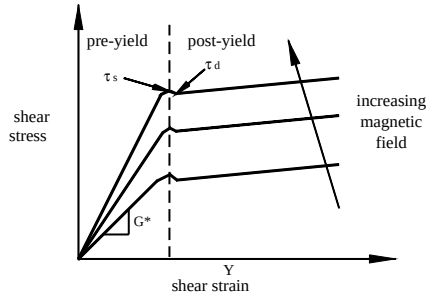

Fig. 1. Shear stress–shear strain relationship of MR materials.

where G' is storage modulus, G'' is the loss modulus. While the storage modulus is proportional to the average energy stored during a cycle of the deformation per unit volume of the material, the loss modulus is proportional to the energy dissipated per unit volume of the material over a cycle.

To investigate the effects of the magnetic field on the vibration response of the three-layered MR adaptive beam by the energy approach, the relationship between the magnetic field and the shear modulus of the MR materials has to be known. Until now, there is no complete investigation of MR materials rheology in the pre-yield regime. However, approximate relations for the shear storage modulus of MR materials in the pre-yield regime were developed through empirical studies [16]. Reviewing Ginder's study, the storage modulus term of the complex shear modulus is shown to be proportional to the magnetic field strength, but the above study did not present any loss modulus information.

In this section, we analyze the relationship between the magnetic field and the complex shear modulus of the MR materials in the pre-yield regime using oscillatory rheometry techniques. The schematic diagram of the fixture and associated testing apparatus are shown in Fig. 2 The fixed part of the fixture mainly consists of two parallel plates on a base. These two parallel plates formed a cavity with a height of 5 mm. A 3 mm thick, 100 cm^2 area plate attached on the shaker head is inserted into the space between the two parallel plates with an equal gap height from them. This symmetric arrangement should avoid the unwanted coupling between the in-plane and transverse motions of the central plate. This in turn would assure the pure shear straining on the MR material filled in the gaps. The magnetic field is established by applying voltage to electromagnet.

During the test, the power amplifier activates the electro-magnetic shaker with the sinusoidal source generated from the function generation. The axial motion of the central plate provides the shear straining on the MR material filled between the plates. The force transducer measures the corresponding reacted axial force on the fixed plates. The input axial displacement signal and the reacted force signal are recorded in the dynamic signal analyzer. Thus, the associated complex shear modulus of the MR material could be calculated accordingly.

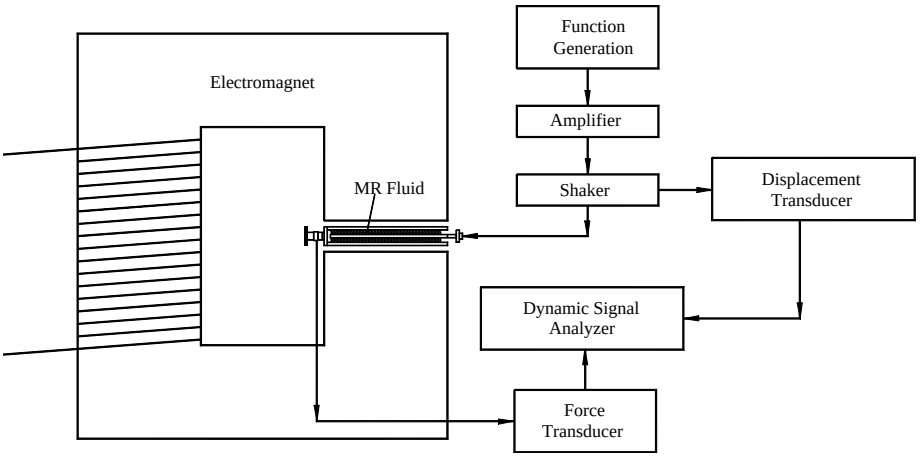

Fig. 2. Schematic diagram of the set-up for the MR fluid under oscillating shear.

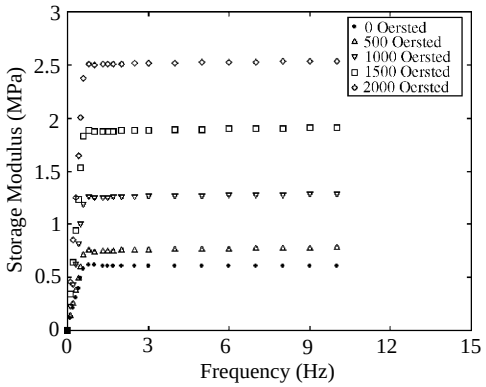

Fig. 3. Storage modulus of MR fluid (measured at various magnetic field strengths and a strain of 0.5%) plotted as a function of frequency.

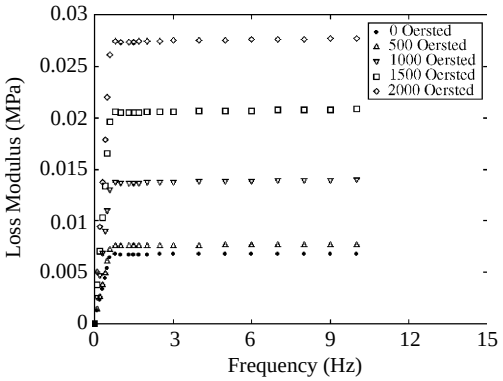

Fig. 4. Loss modulus of MR fluid (measured at various magnetic field strengths and a strain of 0.5%) plotted as a function of frequency.

The data obtained for the MR fluid represent the initial characterization of the pre-yield properties exhibited by this type of material. The increase in the storage modulus and loss modulus can be obtained for the MR fluid by increasing the applied field strength or the frequency as shown in Figs. 3 and 4. In Figs. 3 and 4, when the frequency is higher than 1 Hz, the storage modulus and the loss modulus are only dependent on the magnetic field and the presence of the magnetic field gives rise to larger values of the storage and loss modulus.

Figs. 5 and 6 display the storage modulus and the loss modulus as a function of the magnetic field when the frequency is higher than 1 Hz. Based on the experimental data, the following non-linear relationship between magnetic field and complex shear modulus of the MR materials can be concluded as

$$G^*(B) = G'(B) + \mathrm{i}G''(B), \tag{3}$$

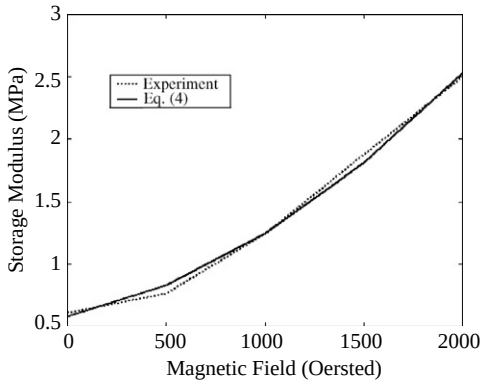

Fig. 5. Storage modulus as a function of the magnetic field.

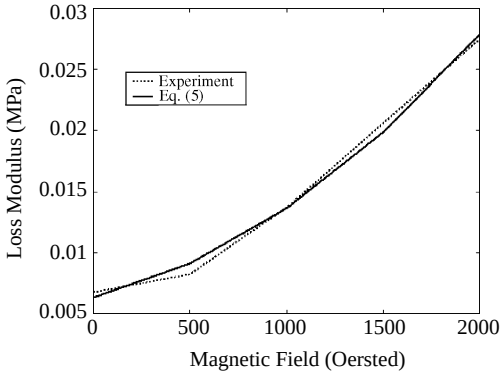

Fig. 6. Loss modulus as a function of the magnetic field.

where

$$G'(B) = 3.11 \times 10^{-7}B^2 + 3.56 \times 10^{-4}B + 5.78 \times 10^{-1}, \tag{4}$$

$$G''(B) = 3.47 \times 10^{-9}B^2 + 3.85 \times 10^{-6}B + 6.31 \times 10^{-3}, \tag{5}$$

where B(oersted) is the magnetic induction.

3. Model and results of MR adaptive beam

The dynamic vibration response modelling of three-layered MR adaptive beams are presented in this section. The Hamilton principle is applied to constitute the model. The configurations of the modelled beams consist of MR material between two aluminum strips. Aluminum strips are approximated as a purely elastic material. MR material is considered as a linear viscoelastic material. Sinusoidal excitation force acting at a single location in the transverse direction on the beam is assumed. The vibration responses including mode shapes, natural frequencies and loss

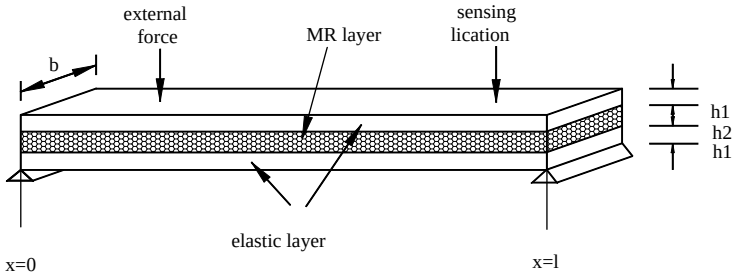

Fig. 7. Three-layered adaptive beam configuration with MR material situated in the middle layer.

factors for different magnetic fields applied over the adaptive beam are predicted. The beam is considered simply supported at both ends. The MR adaptive beam configuration considered in this study is schematically illustrated in Fig. 7.

The assumptions considered in this model are listed as follows. (1) No slipping is assumed between the elastic layers and the MR layer; (2) all three layers experience the same transverse displacement; and (3) no normal stresses in the MR layer and no shear strains in the elastic layers exist.

The governing partial differential equations of the MR adaptive beams are derived using the Hamilton principle that considers the entire motion of the system between two instants t_1 and t_2. The Hamilton principle is invariant with respect to the co-ordinate systems used and is presented in the form

$$\int_{t_1}^{t_2} (\delta T + \delta W)\,\mathrm{dt} = 0, \tag{6}$$

where T is the kinetic energy of the system and W is the work done by external forces between t_1 and t_2. And δ is the operator to define the virtual displacement in the co-ordinates of a system. At low strain levels (less than 1%), the MR material's rheological is in the pre-yield regime and is described by linear viscoelastic theory.

In order to describe the motion equations of the MR adaptive beam by the Hamilton principle, the kinetic energy, potential energy and work done over the beam have to be expressed. The potential energy of the beam includes extensional and bending strain energy of the surface plates and shear strain energy of the MR layer. The final form of the Hamilton principle including the listed terms can be presented as

$$\delta \int_0^{t_1} (T - V_e - V_b - V_s + W)\,\mathrm{dt} = 0. \tag{7}$$

The terms in the above equation are explained as follows: T is the kinetic energy due to transverse and rotational motions, V_e is the potential energy due to extensional stresses of the surface plates, V_b is the potential energy due to the bending stresses of the surface plates, V_s is the potential energy due to the shear stresses of the MR layer, and W is the work done over the adaptive beam by external forces.

The energy terms in Eq. (7) are expressed in the following form:

$$T = \frac{1}{2}\int_0^L \left[\frac{\partial w(x)}{\partial t}\right]^2 \rho(x)\,\mathrm{d}x + \frac{1}{2}\int_0^L \left[\frac{\partial \phi(x)}{\partial t}\right]^2 J(x)\,\mathrm{d}x, \tag{8}$$

$$V_e = \tfrac{1}{4}(h_1 + h_2)^2 b h_1 E_f \int_0^L \left(\frac{\partial \phi}{\partial x}\right)^2 \mathrm{d}x, \tag{9}$$

$$V_b = E_f I_f \int_0^L \left(\frac{\partial^2 w}{\partial x^2}\right)^2 \mathrm{d}x, \tag{10}$$

$$V_s = \tfrac{1}{2} G^* h_2 b \int_0^L \gamma^2\,\mathrm{d}x, \tag{11}$$

$$W = \int_0^L f(x,t) w(x,t)\,\mathrm{d}x. \tag{12}$$

Substituting the energy terms in Eqs. (8)–(12) into Eq. (7) and simplifying, the Hamilton principle takes the form

$$\rho\frac{\partial^2 w}{\partial t^2} + 2E_f I_f \frac{\partial^4 w}{\partial x^4} - G^* b h_2 \left(\frac{\partial^2 w}{\partial x^2} - \frac{\partial \phi}{\partial x}\right) = f(x,t), \tag{13}$$

$$J\frac{\partial^2 \phi}{\partial t^2} - \frac{b h_1 E_f (h_2 + h_1)^2}{2}\frac{\partial^2 \phi}{\partial x^2} - G^* b h_2 \left(\frac{\partial w}{\partial x} - \phi\right) = 0. \tag{14}$$

In the above equations, $w(x,t)$ is the transverse displacement, $\phi(x,t)$ is the cross-sectional rotation, $\gamma(x,t)$is the shear displacement of the MR material, and $\gamma(x,t) = (\partial w(x,t)/\partial x) - \phi(x,t)$, $f(x,t)$is the external force, I_f is the moment of inertia at the centroid of elastic layer, J is mass moment of inertia, E_f is Young's modulus of each surface layer, ρ is the density of the beam cross-section per unit length and b is beam width, h_1 and h_2 are the elastic layer's and MR layer's thicknesses.

Assuming the rotational dynamic is less important than the transverse vibration dynamic, Eq. (14) can be simplified as

$$\frac{b h_1 E_f (h_2 + h_1)^2}{2}\frac{\partial^2 \phi}{\partial x^2} + G^* b h_2 \left(\frac{\partial w}{\partial x} - \phi\right) = 0. \tag{15}$$

For a simply supported boundary condition, the mode shapes are described by sinusoidal wave forms:

$$W_n(x) = \sin(\lambda_n x) \quad (n = 1, 2, \ldots, \infty), \tag{16}$$

$$\Phi_n(x) = C_n \cos(\lambda_n x) \quad (n = 1, 2, \ldots, \infty), \tag{17}$$

where

$$\lambda_n = \frac{n\pi}{L}, \tag{18}$$

and C_n is the ratio of the rotational and transverse displacement amplitudes. Substitution of Eqs. (16) and (17) into Eq. (15) yields

$$C_n = \frac{2G^* h_2 \lambda_n}{E_f h_1 (h_1 + h_2)^2 \lambda_n^2 + 2G^* h_2}. \tag{19}$$

The natural frequencies of the beam under transverse vibration can be calculated by initially assuming a free vibration response of the form

$$w(x,t) = \sum_{n=1}^{\infty} W_n(x) \mathrm{e}^{\mathrm{i}\omega_n t}, \tag{20}$$

$$\phi(x,t) = \sum_{n=1}^{\infty} \Phi_n(x) \mathrm{e}^{\mathrm{i}\omega_n t}. \tag{21}$$

Introducing Eqs. (20) and (21) into Eq. (13), with zero excitation, yields

$$\sum_{n=1}^{\infty} \left[-\rho\omega_n^2 W_n(x) + 2E_f I_f \frac{\mathrm{d}^4 W_n(x)}{\mathrm{d}x^4} - G^* b h_2 \left(\frac{\mathrm{d}^2 W_n(x)}{\mathrm{d}x^2} - \frac{\mathrm{d}\Phi_n(x)}{\mathrm{d}x} \right) \right] = 0. \tag{22}$$

Furthermore, substituting Eqs. (16) and (17) into Eq. (22) results in a complex natural frequency expression given as

$$\omega_n = \sqrt{\frac{2E_f I_f \lambda_n^4 - G^* b h_2 (\lambda_n C_n - \lambda_n^2)}{\rho}}. \tag{23}$$

Then the natural frequency amplitude and the loss factor can be obtained:

$$\omega_n = |\omega_n|(1 + \mathrm{i}\eta), \tag{24}$$

where

$$|\omega_n| = \sqrt{\mathrm{Re}\,\omega_n^2 + \mathrm{Im}\,\omega_n^2}, \tag{25}$$

$$\eta = \frac{\mathrm{Im}\,\omega_n^2}{\mathrm{Re}\,\omega_n^2}. \tag{26}$$

The force vibration responses $w(x,t)$ and $\phi(x,t)$ can be written by the use of expansion theorem as

$$w(x,t) = \sum_{n=1}^{\infty} W_n(x) q_n(t), \tag{27}$$

$$\phi(x,t) = \sum_{n=1}^{\infty} \Phi_n(x) q_n(t). \tag{28}$$

In the above equations, $q_n(t)$ is a time-dependent generalized co-ordinate, $W_n(x)$ and $\Phi_n(x)$ are the transverse and rotational mode shapes corresponding to each natural frequency as described in Eqs. (16) and (17), respectively.

Since the main interest in this study is the transverse vibration response $w(x,t)$, only the expression for transverse vibration in frequency domain will be developed. Substituting Eqs. (27)

and (28) into Eq. (13) results in

$$\sum_{n=1}^{\infty} \sin(\lambda_n x)(\ddot{q}_n(t) + \omega_n^2 q_n(t)) = \frac{f(x,t)}{\rho}. \tag{29}$$

The force vibration responses are evaluated by assuming a point force applied at location $x = x_a$ in the form

$$f(x,t) = \rho F_0 e^{i\Omega t}\delta(x - x_a), \tag{30}$$

where $\delta(\cdot)$ is a δ function, Ω is the actuation frequency, and F_0 is the magnitude of the actuation force.

Multiplying Eq. (29) by $\sin(\lambda_m x)$ and integrating over the beam length including the assumed point force in Eq. (30) result in

$$\int_0^L \sum_{n=1}^{\infty} \sin(\lambda_n x)\sin(\lambda_m x)(\ddot{q}_n(t) + \omega_n^2 q_n(t))\,dx = \int_0^L F_0\delta(x - x_a)e^{i\Omega t}\sin(\lambda_m x)\,dx. \tag{31}$$

From the properties of orthogonality, if $m \neq n$, the integration on the left-hand of Eq. (31) becomes zero, otherwise, Eq. (31) becomes

$$\ddot{q}_n(t) + \omega_n^2 q_n(t) = \int_0^L F_0\delta(x - x_a)e^{i\Omega t}\sin(\lambda_n x)\,dx. \tag{32}$$

Next, one can define function $N_n(t)$ as a generalized force associated with the generalized coordinate $q_n(t)$ in the form

$$N_n(t) = N_n e^{i\Omega t}, \tag{33}$$

where

$$N_n = \int_0^L F_0\delta(x - x_a)\sin(\lambda_n x)\,dx. \tag{34}$$

For a sinusoidal force application

$$N_n = F_0 \sin(\lambda_n x_a). \tag{35}$$

Finally, Eq. (32) can be written as

$$\ddot{q}_n(t) + \omega_n^2 q_n(t) = F_0 \sin(\lambda_n x_a)e^{i\Omega t}. \tag{36}$$

The solution to Eq. (36) is

$$q_n(t) = \frac{F_0 \sin(\lambda_n x_a)e^{i\Omega t}}{\omega_n^2 - \Omega^2}. \tag{37}$$

Substituting Eqs. (37) and (16) into Eq. (27) results in the final expression for the transverse displacement in the time domain

$$w(x,t) = \sum_{n=1}^{\infty} \frac{F_0 \sin(\lambda_n x_a)}{\omega_n^2 - \Omega^2} e^{i\Omega t}\sin(\lambda_n x). \tag{38}$$

In the above equation, n is the mode number of the nth mode shape, $w(x,t)$ is the vibration amplitude at measurement location x and time t.

Table 1
Properties of aluminum and MR material used in the adaptive beam model prediction

Material/data	Density ($g\,cm^{-3}$)	Shear modulus (Mpa)	Elastic modulus (Gpa)
Aluminum	2.7	65.6	70.0
MR	3.5	Eqs. (3)–(5)	NA

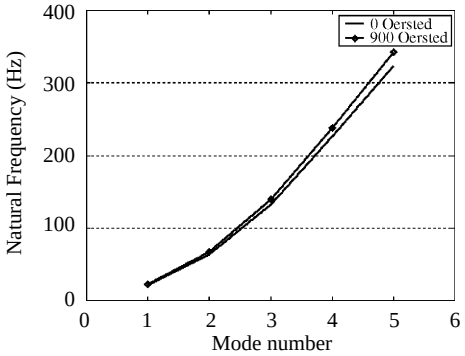

Fig. 8. Effect of the magnetic field on the natural frequencies of the MR adaptive beam.

The predictions of the vibration response of the adaptive MR beam are studied using the developed model. A simply supported beam consisting of two aluminum elastic layers and a MR damping layer sandwiched in between is considered. Theoretical transverse vibration response predictions are obtained using the following beam parameters. The beam is $L = 400$ mm in length and $b = 25$ mm in width. The elastic upper and lower plate material is aluminum, at a thickness of $h_1 = 1$ mm, and the MR material damping layer thickness is $h_2 = 1$ mm. The materials moduli used in the governing equations are given in Table 1.

Fig. 8 illustrates the natural frequency variations of up to five modes. As can be followed from the figure, the natural frequencies shift to higher frequencies as the applied magnetic field increases. This type of response of MR adaptive beams shows strong evidence of controllable capabilities of MR materials in adaptive beams.

Fig. 9 shows the effect of magnetic field on the loss factors of the adaptive beam for the magnetic field levels of 0 and 900 Oe. The loss factors decrease at the first mode and increase at higher modes as the magnetic field strength increases.

Fig. 10 shows the effect of the magnetic field on the vibration amplitude of the MR beam. In the figure, as the magnetic field strength increases, the vibration amplitude of each mode decreases and natural frequencies shift to higher frequencies.

4. Experiments of MR adaptive beam

Experiments are performed to illustrate the controllable capabilities of MR materials in adaptive beams in real time and to verify the theoretical prediction. The geometric shape and

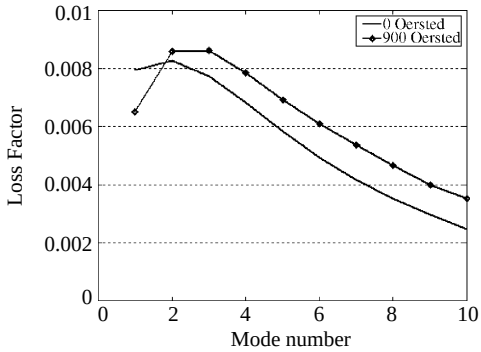

Fig. 9. Loss factor variations for different levels of magnetic field.

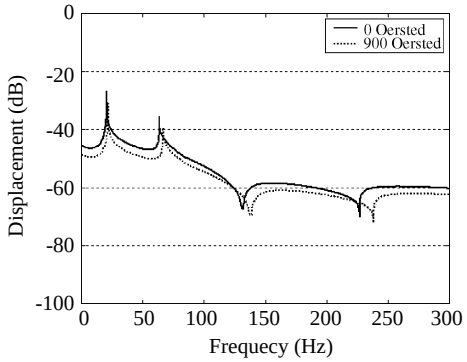

Fig. 10. Transverse vibration response based on different magnetic fields.

mechanical properties of the experimental MR test beams fabricated are the same as those considered in the theoretical model predictions.

In this experimental study, the MR test beam is fabricated according to the following principles: (1) the surface plates must be made of elastic materials, (2) the surface plates should not affect the distribution and strength of the magnetic field, (3) the MR layer should be uniform between the surface plates, and (4) the fabricated MR test beam should be uniform and straight.

The first step of the test beam preparation is the selection of the elastic surface plates. Thin aluminum strips are chosen for this purpose because of its low damping properties and relatively high stiffness properties compared to that of the MR material. Additionally, aluminum has a relative magnetic permeability equal to zero, which indicates that it does not affect the distribution and strength of the magnetic field. The second concern is to keep a uniform gap distribution between the elastic layers in order to have a uniform MR layer. This is maintained by utilizing plastic spacers. 2 mm $\times$ 1 mm plastic spacers are uniformly bonded onto two long edges of one of the aluminum plates. The other aluminum strip is allowed to slide freely on the surface of the spacers. The third step in fabricating the MR adaptive test beam is to seal the edges of the elastic plates in order to keep the liquid MR material inside. Silicone sealant is used for this

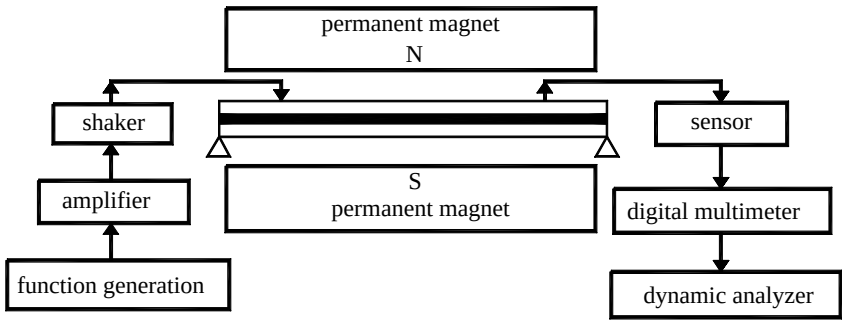

Fig. 11. Experimental set-up.

purpose. Since the silicon sealant is light and flexible, its effect on constraining the motion of the surface plates and MR materials is slight.

After the beam is sealed, the next step is to fill the cavity remaining inside the beam with the MR material. To achieve this, two small holes are left open at each end of the beam. The beam is then held vertical and the MR material is injected into the beam cavity using a hypodermic needle inserted through one hole at the bottom side of the beam. The air existing in the cavity is let out from the other end. This method results in the best filling of the MR beams without empty space left between surface plates.

The experimental set-up is integrated with sensing, actuation and signal analysis equipment as shown in Fig. 11. The instruments used in the experiment include a fiber-optic sensor, shaker, amplifier, function generator, digital multimeter and dynamic analyzer. The functions and properties of each instrument in the experimental set-up are presented as follows. A sensor is used to measure the vibration displacement at a single location. This sensor could sense the displacements from 0 to 10 mm. A shaker generates the excitation force applied over the MR beam. This specific shaker could generate a force up to 4.5 lb with a displacement of 5 mm and a bandwidth from 0 to 10 000 Hz. The shaker is driven by an amplified voltages signal generated by a function generator. A dynamic analyzer is used for the fast Fourier transformation of the acquired analog signals from the fiber-optic sensor. Vibration response in frequency domain, natural frequencies and amplitudes of the vibration are presented in the output of the analysis results. Loss factors are evaluated from the vibration response information in the frequency domain.

Permanent magnets are used to generate magnetic field over the test beam. Variations in the magnetic field level are obtained by changing the distance between the permanent magnets by using a simple screw mechanism. Simple supported boundary conditions are considered. While the original simply supported boundary conditions are horizontal, bending of the beam takes place in the presence of the magnetic field. In order to address this problem, an alternative simply supported boundary condition is designed based on placing the test beam in perpendicular position. The requirements for simply supported boundary condition are satisfied in the design: (1) the transverse displacement should be zero at both ends, (2) the moment should be zero at both ends and (3) the longitudinal displacement is unrestrained. The pins that support the beam are situated in blocks. The blocks have small shallow holes for the pins to fit in. The movements of the

pins are restrained by the holes to satisfy the first requirement of the boundary conditions. The pins could rotate freely in the holes that satisfy the second requirement. One pair of the holes had small grooves allowing the pins in the holes to move along the longitudinal direction and hence satisfying the third requirement of the boundary condition.

Another concern to be addressed here is the magnetic field direction with perpendicular orientation of the beam and the boundary conditions in the experimental study. The model theory developed in the above section considers the magnetic field applied in vertical direction to the beam surface. However, in the experimental study, it is clear that the magnetic field acts along the width of the test beam. Although in this position the magnetic field still changes the rheological properties of the MR material, the complex shear modulus may show slight deviations. Since keeping the beams in a vertical position is the only effective way of carrying out the experiments, this would lead to a level of disagreement with the theoretical results.

The experimental procedure is summarized as follows. First, the shaker tip is glued to the beam at the actuation location that is 220 mm from the left side of the beam. The sensor is located at the point of 80 mm from the right side of the beam with a distance between the sensor tip and the beam of 2 mm.The function generator is set with a swept sine actuation frequency with a range of 0–300 Hz with 1 Hz increments. The voltage amplitude of the actuation signal is 200 mV. The signal output from the function generator is sent to the amplifier and the gain button of the amplifier is adjusted to control the final voltage that is sent to the shaker. Then, the function generator and the amplifier are turned on and the shaker provides the swept sine external vibration over the test beam. The sensor acquires the analog data and the data are sent to the dynamic signal analyzer. The dynamic signal analyzer processes the input signal. The natural frequencies, loss factors and the vibration response in frequency domain of the MR adaptive test specimen are obtained.

The effect of the magnetic field on the vibration response of the MR beam is presented in Fig. 12 for magnetic field levels of 0 and 900 Oe. The 900 Oe magnetic fields is the highest magnetic field level that could be applied by the permanent magnets used in the experimental study. In the figure, as the magnetic field strength increases, the natural frequencies increase; meanwhile the peaks of the curves, representing the vibration amplitudes at natural frequencies, become flatter due to the higher loss factors. Fig. 13 presents the relations between the natural

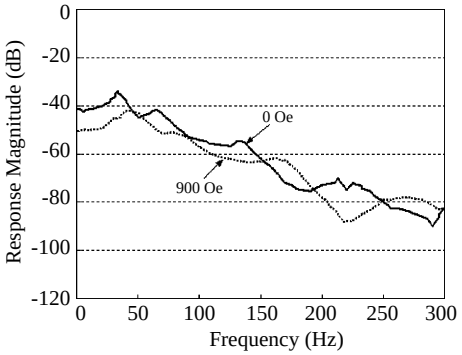

Fig. 12. Experimental loss factors for magnetic field strengths of 0 and 900 Oe.

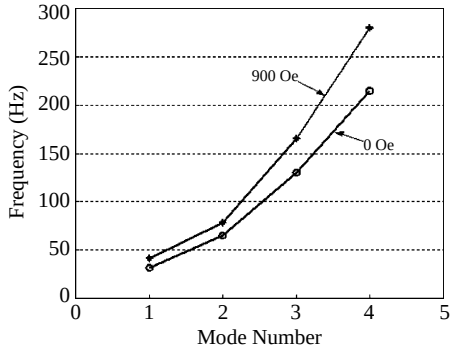

Fig. 13. Experimental natural frequencies for magnetic field strengths of 0 and 900 Oe.

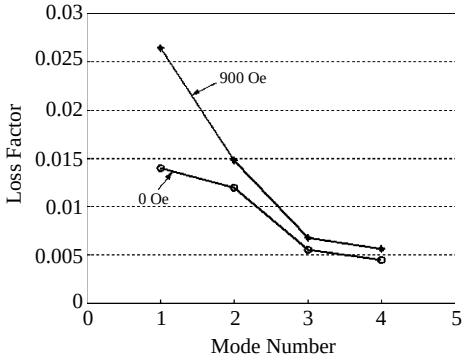

Fig. 14. Experimental loss factors for magnetic strengths of 0 and 900 Oe.

frequencies of the beam and the magnetic field. At the same mode number, a higher magnetic field strength leads to a higher natural frequency of the beam.

The half-power bandwidth relation made the calculations of the structural loss factor from the experimental measurements. This approximation method is based on determining the location of the frequencies corresponding to a 2 dB reduction in vibration response on either side of the vibration peak of a natural frequency. For each mode, the structural loss factor by the half-power bandwidth relation is given as

$$\beta = \frac{\omega_+ - \omega_-}{\omega_n}, \tag{39}$$

where ω_+ and ω_- are the frequencies corresponding to the 2 dB losses, ω_n is the resonance frequency and β is the loss factor of the structure.

The effect of the magnetic field on the loss factors is evaluated in Fig. 14. As the magnetic field strength increases, the loss factors of same mode number increase. This observation is in agreement with the theoretical prediction at higher modes. However, at the first mode the

theoretical prediction based on the energy method illustrated in Fig. 9 shows that a higher magnetic field strength implies a lower loss factor.

5. Conclusions

In this study, the controllable capabilities of MR adaptive beam structures have been investigated. The relationship between the magnetic field and the complex shear modulus of MR materials in the pre-yield regime has been studied using oscillatory rheometry techniques. For MR materials' applications, a theoretical model was developed based on the energy method. From the analysis results, it was observed that MR material presents vibration control capabilities. Vibration amplitudes are decreased with variations in the applied magnetic field for MR material. Furthermore, the natural frequencies shift to higher frequencies when the magnetic field levels are increased. In addition to the model predictions, actual MR adaptive beam was fabricated and tested. Both studies illustrate the vibration minimization capabilities of the MR adaptive beam at different magnetic field levels. But application of magnetic field over the MR layer is becoming an important design criterion in using MR adaptive structures, it can be quite a challenging task to generate a magnetic field over a MR layer.

Acknowledgements

This work was funded by the National Science Foundation (59875068) and Science Foundation (2001SL10) of Shaanxi Province in China. Funding was also provided by the National Education Ministry Foundation of China.

References

[1] S.B. Choi, B.S. Thompson, M.V. Gandhi, An experimental investigation on the active-damping characteristics of a class of ultra-advanced intelligent composite materials featuring electro-rheological fluids, in: L.C. Rogers (Ed.), Proceedings of Damping 89, 1989, Wright Aeronautical Laboratories, Wright-Patterson Air Force Base, OH, pp. CAC1–CAC14.

[2] M.V. Gandhi, B.S. Thompson, Dynamically-tunable smart composites featuring electro-rheological fluids, in: E. Udd (Ed.), Fiber Optic Smart Structures and Skins 2, Vol. 1170, SPIE, Boston, MA, 1989, pp. 294–304.

[3] Y. Choi, A.F. Sprecher, H. Conrad, Vibration characteristics of a composite beam containing an electrorheological fluid, Journal of Intelligent Materials Systems and Structures 1 (1990) 91–104.

[4] Y. Choi, A.F. Sprecher, H. Conrad, Response of electrorheological fluid-filled laminate composites to forced vibration, Journal of Intelligent Materials Systems and Structures 3 (1992) 17–29.

[5] M.J. Mahjoob, H.R. Martin, F. Ismail, Distributed vibration control using electrorheological fluid, Proceedings of the International Modal Analysois Conference, Florida, 1993.

[6] W. Kordonsky, A. Matsephuro, S. Demchuck, Z. Novikova, Electrorheological fluid-based composite materials properties for vibration control in distributed system, in: C.A. Rogers, G.G. Wallace (Eds.), Proceedings of the Second International Conference on Intelligent Materials, Williamsburg, VA, 1994.

[7] D. Ross, E.E. Ungar, E.M. Kerwin, Jr., Damping of plate flexural vibration by means of viscoelastic laminae, Structural Damping, American Society of Mechanical Engineers, section 2, 1959.

[8] C.D. Rahn, S. Joshi, Modeling and control of an electrorheological sandwich beam, American Society of Mechanical Engineers, Design Engineering Division, Publication DE 75, 1994, pp. 159–167.
[9] S.O. Oyadiji, Applications of electrorheological fluids for constrained layer damping treatment of structures, Journal of Intelligent Materials Systems and Structures 7 (1996) 541–549.
[10] C.D. Berg, L.F. Evans, P.R. Kermode, Composite structure analysis of a hollow cantilever beam filled with electro-rheological fluid, Journal of Intelligent Materials Systems and Structures 7 (1996) 494–502.
[11] M. Yalcintas, J.P. Coulter, An adaptive beam model with electrorheological material based applications, Journal of Intelligent Materials Systems and Structures 6 (1995) 498–507.
[12] M. Yalcintas, J.P. Coulter, Electrorheological material based adaptive beams subjected to various boundary conditions, Journal of Intelligent Materials Systems and Structures 6 (1998) 700–717.
[13] D.J. Mead, S. Markus, The forced vibration of a three layer damped sandwich beam with arbitrary boundary conditions, Journal of Sound and Vibration 10 (1969) 163–175.
[14] Y.K. Park, S.B. Choi, Vibration control of a cantilevered beam via hybridization of electro-rheological fluids and piezoelectric films, Journal of Sound and Vibration 225 (2) (1999) 391–398.
[15] S.B. Choi, J.W. Seo, J.H. Kim, K.S. Kim, An electrorheological fluid-based plate for noise reduction in a cabin: experimental results, Journal of Sound and Vibration 239 (1) (2001) 178–185.
[16] J.M. Ginder, Rheology controlled by magnetic fields, Encyclopedia of Applied Physics 16 (1996) 487–503.